PAPER

A biomimetic fish finlet with a liquid metal soft sensor for proprioception and underwater sensing

To cite this article: Sun Wenguang *et al* 2021 *Bioinspir. Biomim.* **16** 065007

Bioinspiration & Biomimetics

PAPER

A biomimetic fish finlet with a liquid metal soft sensor for proprioception and underwater sensing

RECEIVED
30 April 2021

REVISED
16 August 2021

ACCEPTED FOR PUBLICATION
27 August 2021

PUBLISHED
12 October 2021

Sun Wenguang[1,4], Wang Gang[1,4], Yuan Feiyang[1], Wang Siqi[1], Zheng Qiao[1], Wang Kuang[1], Fei Pan[1], Junzhi Yu[2] and Wen Li[1,3,*]

[1] School of Mechanical Engineering and Automation, Beihang University, Beijing 100191, People's Republic of China
[2] The State Key Laboratory for Turbulence and Complex Systems, Department of Advanced Manufacturing and Robotics, BIC-ESAT, College of Engineering, Peking University, Beijing 100871, People's Republic of China
[3] Beijing Advanced Innovation Center for Biomedical Engineering, Beihang University, Beijing, 100191, People's Republic of China
[*] Author to whom any correspondence should be addressed.
[4] These authors contribute equally to this work.

E-mail: liwen@buaa.edu.cn

Keywords: liquid metal printing, proprioception, environment perception, finlet, flow sensing

Supplementary material for this article is available online

Abstract

Finlets have a unique overhanging structure at the back, similar to a flag. They are located between the dorsal/anal fin and the caudal fin on the sides of the body. Until now, the sensing ability of finlets has not been well understood. In this paper, we design and manufacture a biomimetic soft robotic finlet (48.5 mm long, 30 mm high) with mechanosensation based on printed stretchable liquid metal sensors. The robotic finlet's posterior fin ray can achieve side-to-side movement orthogonal to the anterior fin ray. A flow sensor encapsulating a liquid metal sensor network enables the biomimetic finlets to sense the direction and flow intensity. The stretchable liquid metal sensors mounted on micro-actuators are utilized to perceive the swing motion of the fin ray. We found that the finlet prototype can sense the flapping amplitudes and frequency of the fin ray. The membrane between the two orthogonal fin rays can amplify the sensor output. Our results indicate that the overhanging structure endows the biomimetic finlet with the ability to sense external stimuli from stream-wise, lateral and vertical directions. We further demonstrate, through digital particle image velocimetry experiments, that the finlet can detect a Kármán vortex street. This study lays the foundations for exploring the environmental perception of biological fish fins and provides a new approach for the perception of complex flow environments by future underwater robots.

1. Introduction

Fish finlets are small (midspan finlet length 5–18 mm), non-retractable fins located between the dorsal/anal fins and caudal fin of high-performance fish such as tuna and mackerel (figure 1(a)) [1]. A tuna's finlets have a triangular shape, with the front fin ray standing upright and the posterior fin ray overhanging like a flag; the fin membrane is located between the two fin rays (figure 1(b)) [1–3]. Three pairs of muscles that attach to the base of each finlet can actively control the side-to-side swing of the finlet (figures 1(c) and (d)) [1]. Previous studies have revealed several hydrodynamic advantages of finlets for fish swimming. For example, the finlets can redirect the transverse flow to decrease drag [1, 2], strengthen the vortex of the caudal fin to contribute to thrust [3–5] and even reduce the lateral forces and yaw torques during swimming [6].

Fish fins also play an essential role in sensing during fish swimming. Previous studies have revealed that neural networks are distributed in the fin membrane and fin rays of the pectoral and adipose fins [7–10]. For example, the adipose fin can perceive its movement to modulate the fin and control the thrust force during swimming [11–13]. The pectoral fins can help bluegill sunfish sense the surrounding environment by touching obstacles in environments with low or no visibility [14–16]. Ono *et al* stated that sensory nerves are located at the base of or around finlet muscles [17, 18]. Although these nerves are hypothesized to provide proprioception and flow sensing for the finlets, there is no detailed anatomical description or any quantitative physical data so far. In this

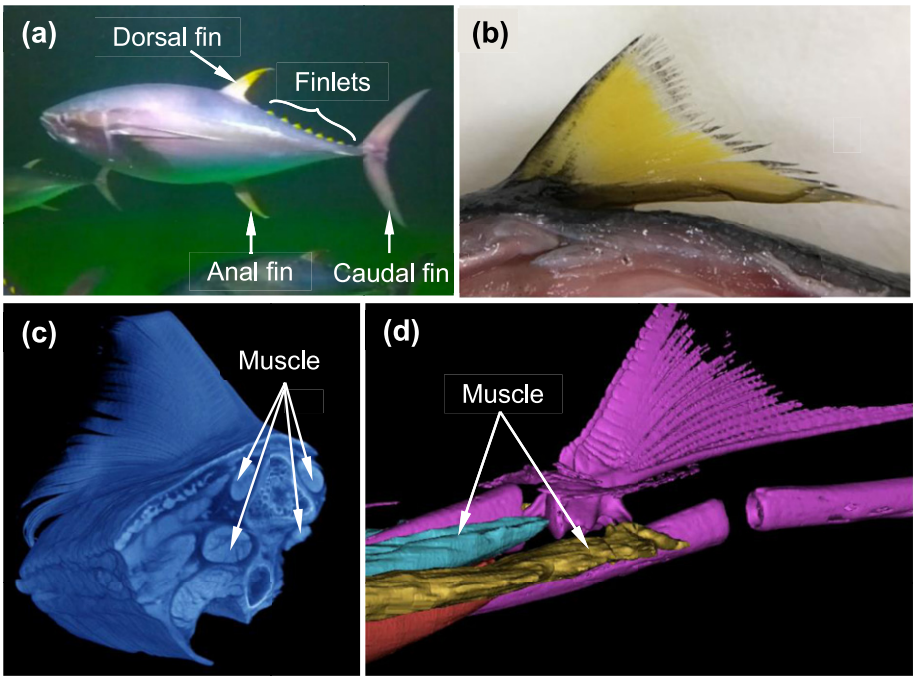

Figure 1. Morphology of biological fish finlets. (a) Yellowfin tuna (*Thunnus albacares*) with finlets located between the dorsal/anal fin and caudal fin. (b) Morphology of a single finlet showing the attached base and the overhand structure. Reproduced from [6]. © IOP Publishing Ltd. All rights reserved. (c), (d) The cross-section of a single fish finlet micro-CT scan with muscles and soft tissues. Reproduced from [5] with permission of The Royal Society of Chemistry.

study, we hope to test this hypothesis robotically by developing a biomimetic robotic finlet. Implementing an at-scale biomimetic finlet with biologically relevant sensors would allow repeatable experiments and the study of underwater sensing and perception. A robotic finlet is also a promising scientific tool for investigating the proprioception and hydrodynamics of finlets during different fish swimming kinematics (such as amplitude and frequency).

Finlets have a unique overhang structure and a soft membrane between two fin rays, which are interesting morphological features. Creating a biologically analogous robotic finlet with morphing and sensing ability is challenging as it combines structural design, actuation, sensing and fabrication from multiple materials within a confined space.

With the development of functional soft materials, flexible sensors have attracted growing attention and have been applied to bio-inspired systems due to their compactness, stretchability and sensitivity [19–26]. For example, bio-inspired soft sensors for sensing air and water flow have been developed by mimicking mammalian whiskers based on the principle that the electrical resistance of soft materials changes in response to external forces [27–29]. The lateral line system of fish has inspired various underwater flow sensors. Artificial lateral line sensors have been developed based on sensing principles such as piezoelectric, piezoresistive and capacitive effects [30–33]. However, very few studies have reported robotic models that mimic finlet morphology with a biologically relevant structure, actuation and sensing.

In this work, we aim to implement a biomimetic soft robotic finlet that integrates structure, actuation and soft sensing. We will then explore its locomotion and the perception performance in aquatic environments. We first describe the fabrication of small-scale, printed liquid metal flexible sensors that can sense external forces in different directions. Then, we introduce the implementation of the biomimetic robotic finlet that can realize multimodal movement and integrate it with flexible sensors to realize integration of both swinging and sensing. Finally, we built an experimental apparatus to test the motion and perception functions of the biomimetic robotic finlet. In this work, we focus on using the biomimetic prototype to provide new insights for underwater robot sensing

2. Material and methods

2.1. Bio-inspired robotic fish finlet

Our robotic prototype was inspired by the finlets of yellowfin tuna (*Thunnus albacares*) [5]. Each tuna finlet has three pairs of muscles (figures 1(c) and (d)). Selection of materials for the robotic fin ray was based on the biological study of live tuna fish [34]. Fish fin rays in different regions have different mechanical properties. Research has shown that the Young's modulus of fin rays varies from 0.24 to 3.7 GPa in a single species [34]. Our robotic finlet used 3D-printed

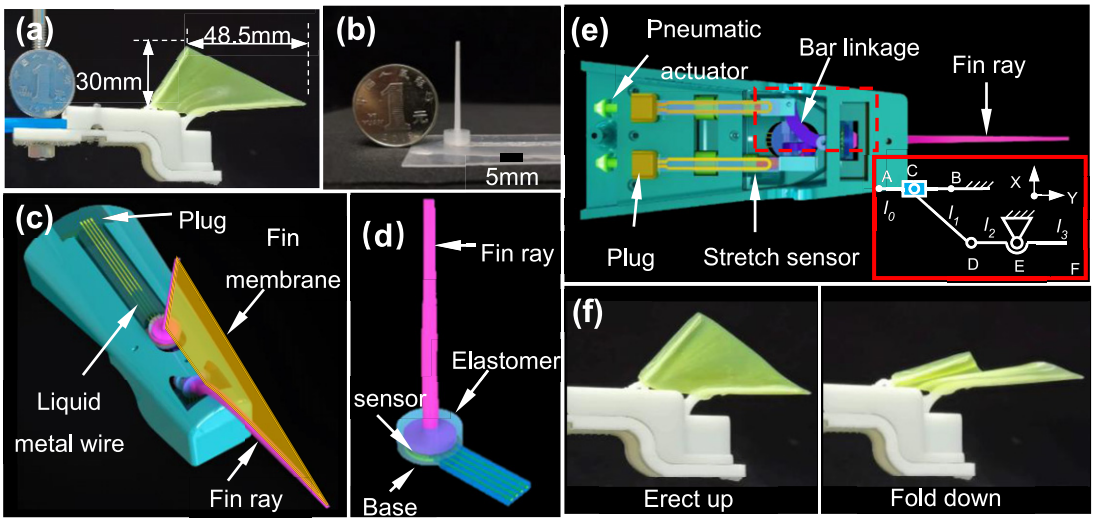

Figure 2. The soft robotic finlet prototype. (a) A photo of the robotic finlet prototype. (b) A fin ray with a liquid metal flow sensor (scale bar 5 mm). (c) Computer-aided design (AD) model of a robotic fish finlet. The silicone membrane is glued onto two fin rays. The posterior fin ray can achieve side-to-side movement using a pneumatic cylinder. The liquid metal wire connects the fin ray sensor to a breakout board connecting the conductive wire to the micro-controller. The plug is a chunk of soft material which seals the end of the finlet structure. (d) CAD model of the fin ray sensor. The fin ray is embedded in the silicone elastomer with the soft sensor underneath. (e) Bottom view of the robotic fish finlet CAD model. The pneumatic actuator (pneumatic cylinder) allowed us to achieve linear movement of 5 mm. The linear movement triggers the bar linkage mechanism to transform the linear motion to posterior fin ray rotation. A stretch sensor is used to realize proprioception. A plug is applied to secure the pneumatic actuator into place. (f) Biomimetic soft finlet in fully erected (500 kPa) and fully folded down (0 kPa) states.

polylactic acid (Young's modulus 1.7–3 GPa) as the fin ray material, which is within the modulus range of a live fish fin ray. We used a type of silicone elastomer (Ecoflex 00-30, Smooth-On, Inc.) for the fin membrane. The robotic finlet was composed of two highly compact flow-sensing fin rays, two bar-linkage mechanisms powered by a pneumatic actuator with proprioception ability, a 3D-printed structure and a soft fin membrane (figures 2(a), (c) and (e)).

The rigid structure was designed on the basis of the morphology of tuna finlets, and its dimensions were within the range of those of tuna finlets. We applied silicon rubber adhesive (Smooth-on Sil-Poxy) to the soft fin membrane to hold the soft membrane on the fin rays. The flow sensor was placed under each fin ray, including both anterior and posterior fin rays (figures 2(b) and (d)). Each sensor could detect forces from three different directions.

The robotic finlet can achieve two types of movement. The folding mechanism allows the anterior fin ray to fold down/become erect (figure 2(f)). The folding movement allows morphing to change the area of the fin that interacts with water. Having this function may benefit the swimming and maneuvering of the fish. The oscillating mechanism allows the posterior fin ray to rotate from side to side. The oscillatory mechanisms needed to realize a rotation of 120° at the posterior fin ray in a confined space and the power source must be small enough to fit in our robotic finlet model. The pneumatic actuator was powered by a micro-pump (OB1, Elveflow, France) through a mini cylinder with a diameter of 3.5 mm. A detailed description of the bar linkage is given in section 2.3.

The finlet prototype has two main sensing functionalities. The first is the finlet flow sensor used to sense three-dimensional flow. The second is the stretchable sensor for proprioception. The proprioception sensor was used to measure the side-to-side movement of the finlet. Both sensors were fabricated using liquid metal printing technology.

2.2. Finlet flow sensor: fabrication and characterization

The flow sensor was designed to sense three-dimensional flow waves. Considering the need for sensitivity, elasticity and waterproofing, liquid metal was used as the conductive element in our flow sensor; it was covered with silicone elastomer to give a waterproof outer layer. Each flow sensor consists of three resistance pressure patterns which are 360° divided into three equal pieces (figures 3(b) and (c)). This type of pattern design can detect the signal amplitude of the incoming flow and detect its direction by considering the signals from all the sensors.

The principle of the flow sensor is as follows: when pressure is applied to the sensor, the liquid metal micro-channels deform so that the resistance of the liquid metal changes. The original change in the resistance is small. Two methods were used to amplify the resistance signal of the flow sensor. The first was a physical method that used a rigid fin ray seated on the flow sensor. When the fin ray bent, it would apply forces to the three pressure patterns. The second method for amplifying the signal involved implementing a signal amplifying circuit, which amplifies the resistance signal using a differential amplifier. This

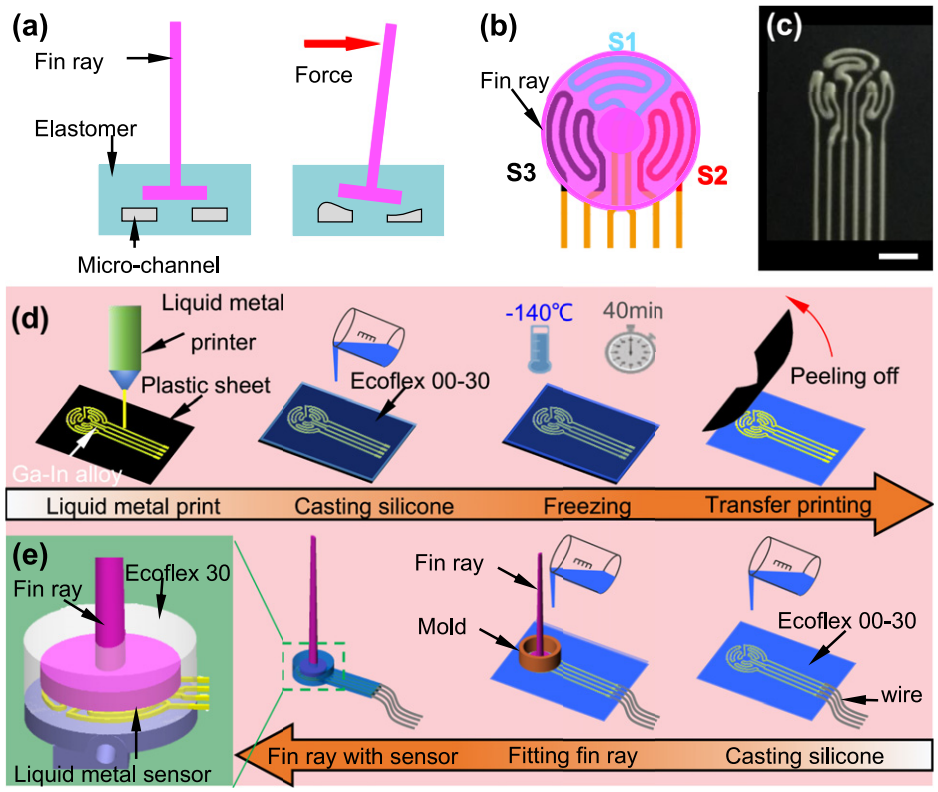

Figure 3. Schematic view of the fabrication of the soft sensor. (a) The working principle of the flow sensor. The liquid metal (eGaIn) pattern was printed and transferred onto the silicone elastomer. When the fin ray bends, the liquid metal micro-channel deforms, which results in a resistance change. (b) Liquid metal pattern. Three micro-channels at 120° intervals allowed us to detect forces from three different directions. The pink transparent circle represents the rigid base of the fin ray, and the solid pink circle represents the head of the fin ray. (c) Photo of a liquid metal pattern (scale bar 3 mm). (d) Fabrication of the flow sensor. (e) Close-up view of the liquid metal flow sensor.

allowed us to amplify the signal with a tuned amplifying parameter. The sensor data can be measured by our data-gathering circuit, consisting of a signal amplifying circuit and an Arduino board, which transmits the sensor data to our computer via serial communication.

Figure 3(d) shows the process for fabricating the flow sensor. We first printed liquid metal (eGaIn) on a plastic film using a liquid metal printer (Dream-Inc Inc., China). Next, we poured silicon elastomer (Ecoflex 00-30) onto the printed substrate and waited for it to cure. Then, in a low-temperature fridge, the eGaIn was transferred onto the soft substrate at a temperature below −140 °C for 40 min. After that, we manually soldered a flat wire socket with wire onto the liquid metal with a soldering kit and poured on another layer of silicone elastomer (Ecoflex 00-30) to cover the surface of the liquid metal. After curing, a 3D-printed ring was put on top of the flow sensor and the fin ray was secured with silicone elastomer (Ecoflex 00-30), which was then cured. Finally, the ring was removed and the sensor cut to shape, as illustrated in figure 3(e).

After the fabrication of the flow sensor, the sensor was characterized. Experiments were conducted to push the tip of the fin ray to characterize the effectiveness, linearity and multi-directional sensing ability of the sensor. The sensor signal and applied force signal were measured simultaneously. The sensor signal was measured with an Arduino Mega 2560 board. The force signal was measured with a multi-axis ATI Delta force transducer (Delta, ATI industrial, Inc.). An industrial robotic arm (Motoman MH3F, Yaskawa Inc., Japan) was applied to linearly push the tip of our fin ray to produce pressure on the flow sensor. The velocity and displacement of the movement were controlled by a programmable robotic arm. Pushing the fin ray applied a pressure that caused the liquid metal channel to deform; the subsequent change in the sensor's resistance was gathered by a micro-controller with an amplifier circuit. We conducted experiments for all six directions and selected three typical cases to show the feasibility of the flow sensor. Furthermore, we explored how the length of the fin ray influenced the sensor output. Each experiment was repeated five times. A Butterworth filter filtered the data to eliminate the noise. The results in the figures only show one of the datasets.

After characterizing the flow sensor, we mounted the sensor onto the prototype and added a soft membrane which was stuck onto both the anterior and posterior fin rays using silicon rubber adhesive. Then an experiment was conducted to measure how the two

sensors work to detect a force. We simulated the force using water flow creating by a hydraulic pump and a section of water tube. The pump could provide a force of ∼100 mN under water; the direction of the force is illustrated by the black arrow in figure 8(b).

2.3. Robotic finlet modeling: kinematics and proprioception

A pneumatic system powered morphing and swinging of the robotic finlet posterior fin ray. Each mini cylinder provided a 5 mm piston movement. One of these linear movements allowed us to power a four-linkage mechanism with an end-effector rotation of 120°. The other helped to achieve morphing, allowing the anterior fin ray to fold down/become erect.

Our design schematic of the planar four-bar linkage is shown in figure 2(e) in the bottom right corner; the slider C moves along the direction of the y-axis producing rotation of the posterior fin ray tip. Our coordinate system O–XY merely displays the x-axis and y-axis directions rather than the position. The cylinder fixed on the finlet base can provide a linear movement from point A to point B for slider C. Point D denotes a revolving joint without any positional constraints. Point E denotes a revolving joint fixed on the finlet base, and point F denotes the tip of the posterior fin ray. When slider C moves from point A to point B, the length of segment AC increases; its value ranges from 0 mm to 5 mm.

The origin of our coordinate system was assigned to point A. l_1, l_2 and l_3 denote the lengths of bars CD, DE and EF, respectively. The kinematic equation is as follows:

$$x(l_0) = (x_F, y_F), \tag{1}$$

where l_0 denotes the length of segment AC and coordinate (x_F, y_F) denotes the position of fin ray tip F, which represents the end-effector. The kinematic equation can be solved using the following expressions:

$$\begin{cases} (x_D - x_C)^2 + (y_D - y_C)^2 = {l_1}^2 \\ (x_D - x_E)^2 + (y_D - y_E)^2 = {l_2}^2 \\ x_F = \dfrac{l_2 x_D + (l_2 + l_3)(x_E - x_D)}{l_2}, \\ y_F = \dfrac{l_2 y_D + (l_2 + l_3)(y_E - y_D)}{l_2} \end{cases} \tag{2}$$

where l_1 and l_2 denote the length of segments CD and DE, respectively, coordinate (x_C, y_C) denotes the position of slider C, coordinate (x_D, y_D) denotes the position of revolving joint D and coordinate (x_E, y_E) denotes the position of revolving joint E. The parameters of this linkage were measured and are listed in table 1.

Using the argument l_0, known parameters and the equations above, we can solve the position of the fin ray tip F, denoted by (x_F, y_F).

Table 1. Parameters of the linkage.

Symbol	Value	Description
l_1	10 mm	Length of segment CD
l_2	2.23 mm	Length of segment DE
x_A	0	Origin point A
y_A	0	Origin point A
x_C	0	Position of slider C
y_C	l_0	Position of slider C
x_E	7.79	Position of revolute joint E
y_E	11.3	Position of revolute joint E

Experiments on finlet motion were conducted to measure the ability to move. Finlet movement was implemented by an integrated pneumatic system (OB1, Elveflow, France) which provides a sine signal of the pressure with an amplitude of 0.5 bar and a frequency of 1–5 Hz. The fixed parameter was pressure signal amplitude, which was maintained at 0.5 bar. The controlled parameter was the pressure signal frequency, which was changed from 1 Hz to 5 Hz in intervals of 1 Hz. Previous work has shown that area of the fin influences the swimming of the fish [46]. The same principle applies to the folding mechanism. Morphing is an additional function that allows us to investigate how the ability of the finlet to morph affects its swimming efficiency.

A liquid metal stretch sensor (proprioception sensor) was designed to sense the finlet's movement. The difference is the pattern of the liquid metal, which does not require the fin ray to be in contact with the sensor. Two experiments were conducted to characterize the proprioception sensor. The first characterized the relationship between the measured resistance and the length change. A robotic arm stretched the proprioception sensor to a certain displacement (20 mm). This experiment was repeated five times. The results show the calculated mean value of data from all five experiment results. The second was a repeating test which also used a programmable robotic arm for repeated movement. We programmed the robotic arm to move from a designated point of origin to a linear displacement of 20 mm as in the first experiment without stopping, and the movement was repeated 75 times. The motion-sensing principle of the finlet is shown in figure 2(e). The flexible stretch sensor is fixed on the pneumatic actuator. When the actuator moves, the stretch sensor stretches along with the driver, resulting in a change in resistance. According to the relationship between resistance and tensile displacement (figure 7(a)), one can calculate the displacement of the actuator. The actuator is connected to the fin via a crank slider mechanism (figure 2(e)), and the angle of swing of the fin can be obtained according to equation (2).

A proprioception experiment was conducted to validate proprioceptive ability. The finlet moved under a sinusoidal pressure with a pressure amplitude of 0.5 bar and frequency of 3 Hz. Meanwhile,

the proprioception sensor data and high-speed camera images were collected. We used high-speed camera images to calculate the pitch angle. Comparing the kinematic modeling with the proprioception sensor data, one can compare sensor data-based finlet kinematics with the finlet kinematics calculated from the images.

Furthermore, we performed two experiments to show the benefits of the soft fin membrane. We first compared the sensory outputs of two biomimetic finlets (with and without a soft membrane) under the actuation of swinging side to side at amplitudes of 28 mm and a frequency of 3 Hz. Then we compared the sensory data for both biomimetic finlets (with and without a soft membrane) encountering a jet flow with a velocity that increased from 0 m s^{-1} to 0.22 m s^{-1}.

2.4. Hydrodynamic and sensing characterization of the robotic finlet

We used the digital particle image velocimetry (DPIV) method to investigate the hydrodynamic function of our robotic finlet (for a detailed introduction to particle image velocimetry see [35–40]). Our experiment was conducted on an integrated experimental apparatus constructed as follows: the robotic finlet with a wired connection was installed in a loop water tank with a metal stick that transforms the force to a force transducer. The signal wire connected the robotic finlet to a PC through a micro-controller (Arduino) to gather sensor data. The force transducer was mounted on a fixed aluminum frame connecting to a PC through a DAQ card (PCI-6284, National Instrument Inc., USA). A pneumatic system (OB1, Elveflow, France) was used to control the air pressure to the finlet cylinder. An air pump powered the pneumatic cylinder. A high-speed camera was installed below the water tank, and a laser system pointed to the front of the tank glass to create a laser sheet with green light. When particles (10 μm average size glass microspheres) were seeded to the water, the laser light sheet would light up the particles. A high-speed camera captured particle motion due to hydrodynamic movement.

A 3D printed cylinder with a D-shaped cross-section provides the Kármán vortex street towards the finlet. In this experiment, the speed of the water flow was 117 mm s^{-1}, the diameter of the D-shaped cylinder that produces the Kármán vortex street was 25 mm and the shedding frequency of the Kármán vortex street was 1 Hz. The prototype robotic finlet was positioned 15 mm behind the pillar for an optimal result.

3. Results

3.1. Performance of the soft flow sensor

We measured the force response of the finlets with the liquid metal sensor (figure 4). We used the robotic arm to push the tips of the fin ray from three orthogonal directions and recorded the changes in resistance of three sensors. Figure 4(a) shows that when the force indicated by the arrow is applied to the fin, the resistance of sensor 1 (S1) increases while the resistances of sensor 2 (S2) and sensor 3 (S3) decrease. This is due to the force: the micro-channel of S1 was pressed and the cross-sectional area decreased, leading to an increase in resistance. Meanwhile, the micro-channels of S2 and S3 were stretched, causing the cross-sectional area to increase, thus reducing the resistance. From figure 4(b), when S1 and S2 were pressed, the pressure applied to S2 was greater; thus, the resistance of S2 increased more than that of S1. This is because the sensor placement and the force direction were not aligned. As a result, the direction of the applied force (horizontal from left to right) was not orthogonal to sensor S2. The applied force would simultaneously press the micro-channels of S1 and S2, causing the resistance of the two sensors (S1 and S2) to increase at the same time. Figure 4(c) shows that the forces applied to S2 and S3 were almost identical.

The sensing properties of the soft sensor with the anterior fin ray were then evaluated. A robotic arm pushed the tip of the fin ray to produce a continuous displacement from 0 to 7 mm, and the corresponding changes in resistance were continuously measured and plotted against displacement (figure 4(d)). The relative change in resistance with respect to displacement shows that the resistance change has a linear relationship in the middle region (3–6 mm). When the displacement is more than 7 mm, the sensor's resistance reaches a maximum and then stays constant. More details can be found in supplementary video S1 (https://stacks.iop.org/BB/16/065007/mmedia).

The electro-mechanical properties of the soft sensor were investigated in detail. We measured the resistance of the sensor, and the pushing force was applied by a robotic arm that pushed the fin ray step by step from 1 mm, 2 mm, …, 5 mm (10 s for each step) (figure 4(e)). It can be found that the resistance showed a significant change when the fin ray was pushed; the resistance remained unchanged under the same displacement. Even under a displacement of up to 5 mm (figure 4(e)), the sensor maintained an acceptable response. More details can be found in supplementary video S2.

The length of the fin ray has a notable influence on the sensing ability of the sensor (figure 4(f)). We conducted displacement-sensing experiments on three fin rays of different lengths and found that although the shorter fin rays are more sensitive than the longer one, the perceptible range of displacement is smaller. The medium length fin ray can perceive the environment more sensitively and has an extended measuring range.

Our result shows that the fin membrane could enhance the sensing performance of the sensor

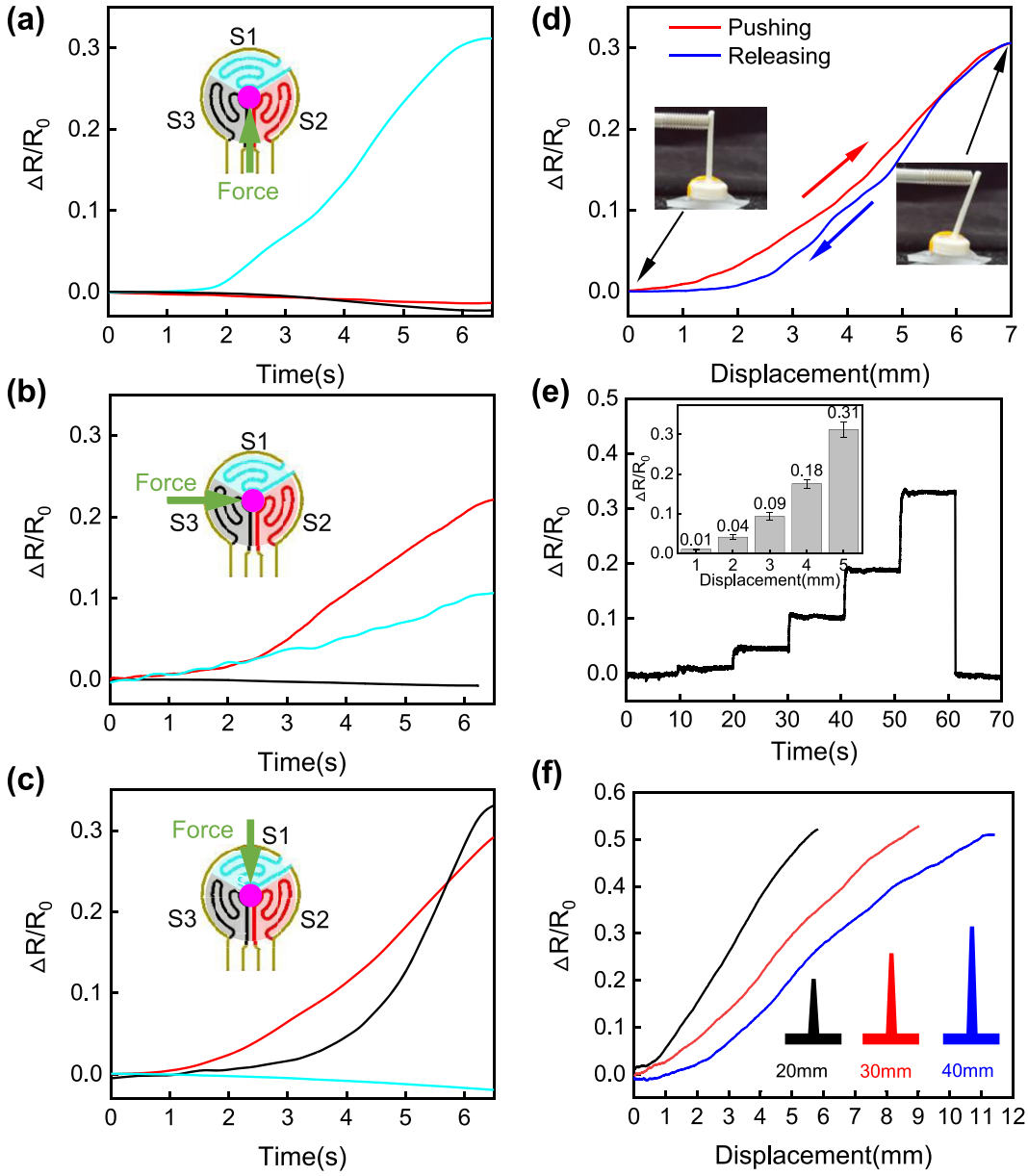

Figure 4. The sensory performance of the soft robotic finlet. The sensor was fixed on a rigid plane. A robotic arm pushed the fin ray tip with a linear movement of 6 mm. (a)–(c) The resistance as a function of time. Different resistance changes resulted from forces with different orientations. (d) The resistance as a function of the displacement of the fin ray tip. The red line represents the sensor resistance for displacement from 0 to 7 mm, and the blue line represents the sensor resistance for displacement from 7 to 0 mm. (e) The value of the resistance during each step of the push. The black curve represents the resistance data. Each step was maintained for 10 s. The inset panel shows the resistance value under different displacements. Error bars are ±1 s.e.m., $N = 5$. (f) The length of the fin ray influences the performance of the sensor.

(figure 5). In the two states of finlet with fin membrane and the one without (figure 5(a)), the performance of the sensor perceiving lateral water flow and swinging motion was tested. In a lateral water flow, the finlet with the fin membrane causes a greater change of resistance (figure 5(b)). With the same principle, the finlet with a fin membrane is more sensitive to swinging motion (figures 5(c) and (d)). The sensory output of the finlet with the membrane is stronger than that of the one without in both experiments, which indicates that the soft membrane can amplify the sensory output of the fin rays.

3.2. Kinematics of the biomimetic robotic finlet

In order to test the kinematics of the finlet, the finlet was driven to oscillate at different frequencies (1–5 Hz) in still water (supplementary video S3). We measured the thrust and side force generated by the finlet via a six-axis force transducer and collected images from the top view by a high-speed camera at a frame rate of 500 frames per second. Figure 6(a) shows sequential photos of the motion of the robotic finlet taken by high-speed camera.

The results show that the amplitude of the finlet swinging gradually decreases as the frequency

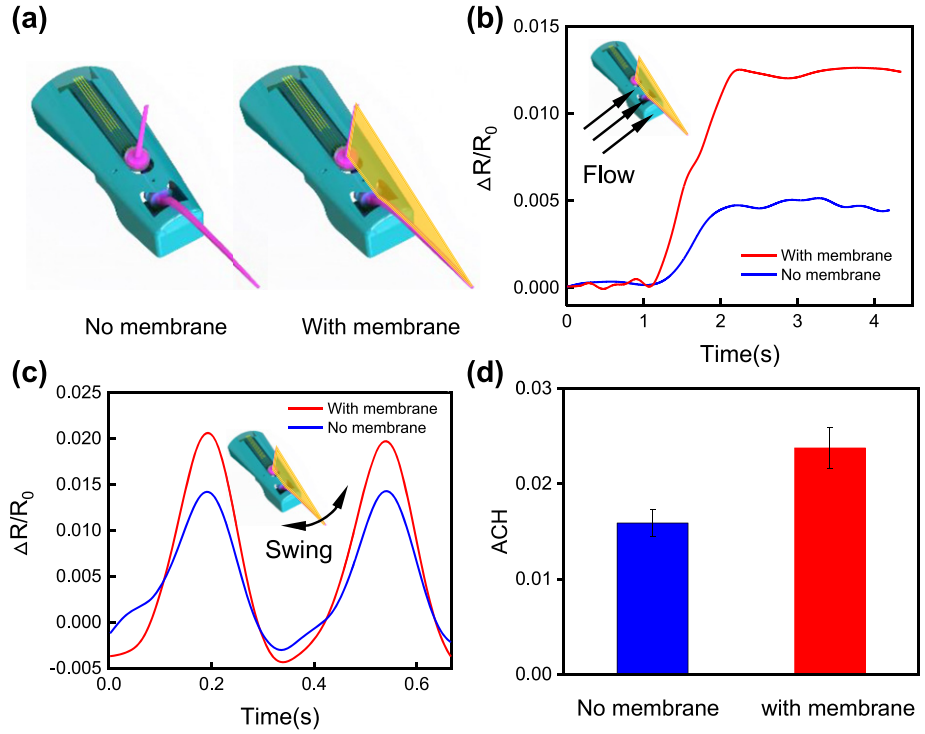

Figure 5. Effect of the membrane on the sensory performance of the robotic finlet. (a) Two CAD models of the finlet which represent two cases in the experimental setup. The left model represents the prototype without a membrane and the right model represent the prototype with a membrane. (b) The sensory outputs of lateral deformation when the finlets (with and without a membrane) encountered a jet flow with a velocity increasing from 0 m s^{-1} to 0.22 m s^{-1}. (c) The sensory outputs of lateral deformation when the finlets (with and without a membrane) actively swing under an actuation of 3 Hz, with an amplitude of 28 mm. (d) Comparing the average cyclic height (ACH) of the sensor value ($\Delta R/R_0$) between the no membrane condition and the with membrane condition. Error bars are ± 1 s.e.m., $N = 5$.

increases from 1 to 5 Hz (figures 6(b)–(d)). The maximum amplitude of the finlet swing from one side to the other is 40 mm (figure 6(b)), and the maximum side-to-side angle is 79.9° at a frequency of 1 Hz (figure 6(e)). When the swinging frequency reaches 5 Hz, the minimum swinging amplitude decreases to 18 mm, and the swinging angle is only 36.4° (figure 6(e)). This decline may be caused by the combination of fluid drag force and the flexible deformation of the soft membrane. No study to date has characterized the thrust force of a biological finlet due to the complexity of testing live tuna *in vivo*. Our robotic experiments show that a finlet with a biologically relevant scale can produce a thrust force of 4.1 ± 1 mN (figure 6(f)). To clarify, the thrust force of 4.1 mN is a time-averaged result which indicate how finlets facilitate swimming. Compared with the thrust force of other appendages of the tuna robot, Zhu *et al* measured that the tuna-inspired robot's caudal fin can produce a thrust force of 100 mN at a swimming frequency of 4 Hz [41]. Comparison of the thrust contribution of finlets and other appendages is less understood and is worth future exploration.

3.3. Proprioception of the biomimetic robotic finlet

In order to test the proprioception of the soft stretch sensor we carried out the experiments to test its linearity (figure 7(a)) and repeatability (figure 7(b)). Figure 7(a) shows that the soft stretch sensor has an excellent linear behavior and can still maintain a linear performance when the maximum stretch rate is 100%. When the flexible sensor is stretched from the original length of 20 mm to 40 mm, the length of the micro-channel increases and the cross-sectional area decreases. According to the characterization of the proprioception sensor, the relationship between the measured resistance and the length change can be calculated through the following formula:

$$\frac{\Delta R}{R_0} = 0.02 l_0 - 0.018.$$

In addition, due to the good circulation and conductivity of the liquid metal, the resistance of the soft stretch sensor keeps increasing linearly. The soft stretch sensor maintained superb response and recovery properties even under an ultrahigh deformation of 100% (figure 7(b)), which may give it a promising future in more precise measurement applications.

The robotic finlet was actuated to swing periodically by a microfluidic pump, while the resistance of the soft stretch sensor was recorded (figure 7(c)). When the finlet swings from one side to the other, the resistance will increase as the soft sensor is stretched. Therefore, the frequency and amplitude of the biomimetic robotic finlet swing can be obtained

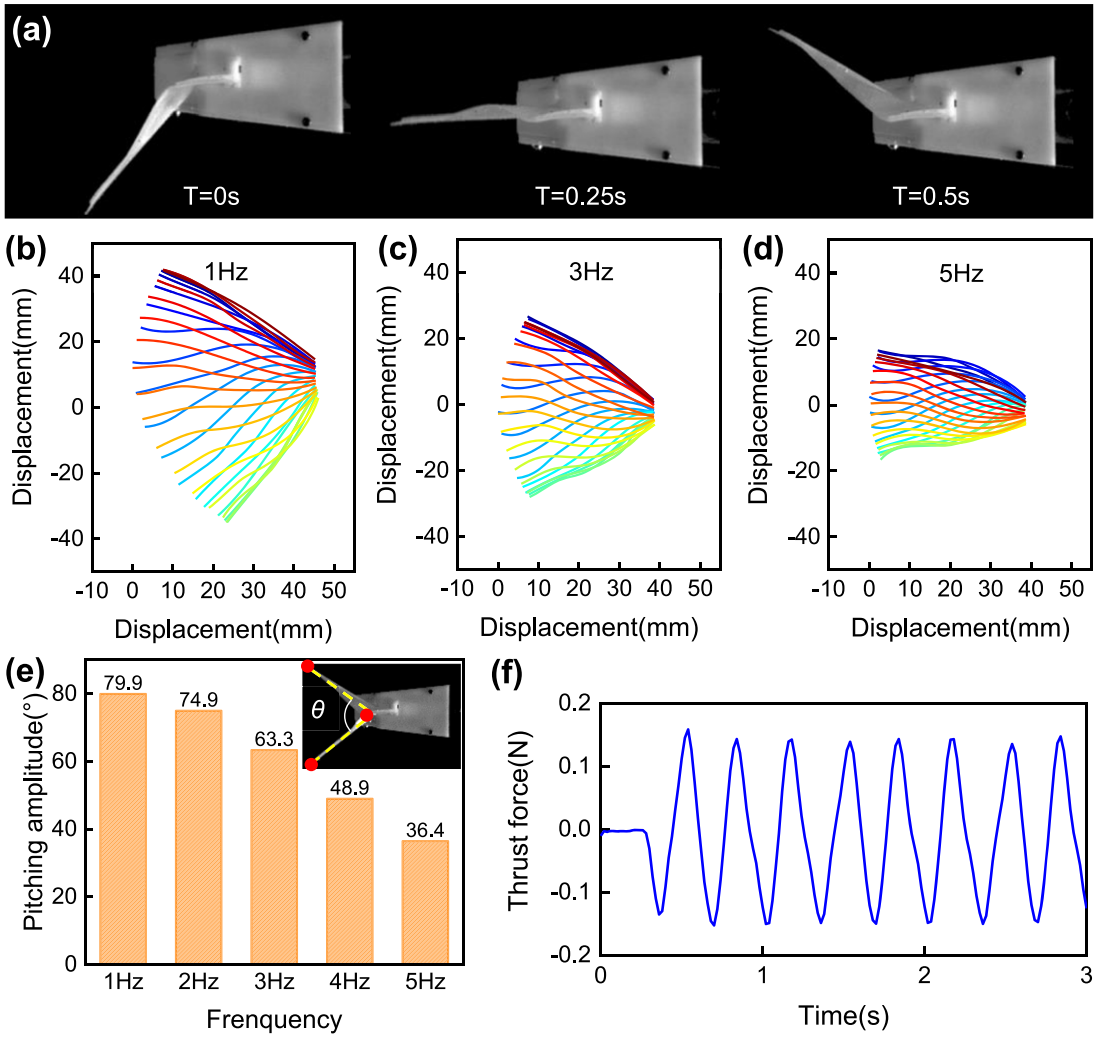

Figure 6. Side-to-side movements of the fin ray at different flapping frequencies. (a) Images of the robotic finlet's movement taken by a high-speed camera. (b)–(d) Side-to-side motion capabilities of the fin ray with different frequencies (1, 3 and 5 Hz) powered by a pneumatic control device providing the air pressure from 0 to 500 kPa. (e) Result of pitching amplitude as a function of the frequency. (f) The result for thrust force with time shows a net thrust force produced by the robotic finlet.

from the feedback of the resistance change data of the stretch sensor. According to the theoretical model based on formula (2), the position of the finlet can be reconstructed using the feedback resistance. Figure 7(d) shows comparisons between experimental (yellow dashed lines) and model reconstructed posterior fin ray profiles of the finlet (purple solid lines). As the swinging angle of the posterior fin ray increases, the error between the reconstructed model and the real-time position of the fin ray is less than 3 mm. Therefore, the real-time position of the fin can be obtained through proprioception (see supplementary video S4).

3.4. Perception of external stimuli by the biomimetic robotic finlet

The response of the finlet to external forces was measured in threeorthogonal directions (x, y, z) in space (figure 8). The robotic finlet has two orthogonally placed fin rays, the anterior and posterior fin rays. Each fin ray has a flow sensor consisting of three resistive sensors distributed in the pattern shown in figure 8(b). Forces was applied from the x, y and z axes to the finlet, as shown in figure 8(a), and the responses of the six resistive sensors were noted. From figure 8(c) we can see that stimulation via external forces in different directions can cause different sensory responses. Firstly (case 1), when the finlet receives a force in the x direction, the resistance of sensor 5 of the interior fin ray increases. However, sensors 1, 2 and 3 of posterior finlet cannot perceive the force from the x axis, so that there is no significance change in resistance. This is because the fin ray was along the x axis. Secondly (case 2), when the finlet receives a force in the y direction, the resistance of sensors 4 and 3 (the principle is shown in figure 4(b)) increases due to the lateral force on both fins. Thirdly (case 3), when the finlet receives a force in the z direction, similar to case 1, only the resistance of sensor 2 of the posterior fin ray increases. The dynamic change in the line graph in figure 8(c) accurately reflects the external stimulus in the three directions (stream-wise, lateral

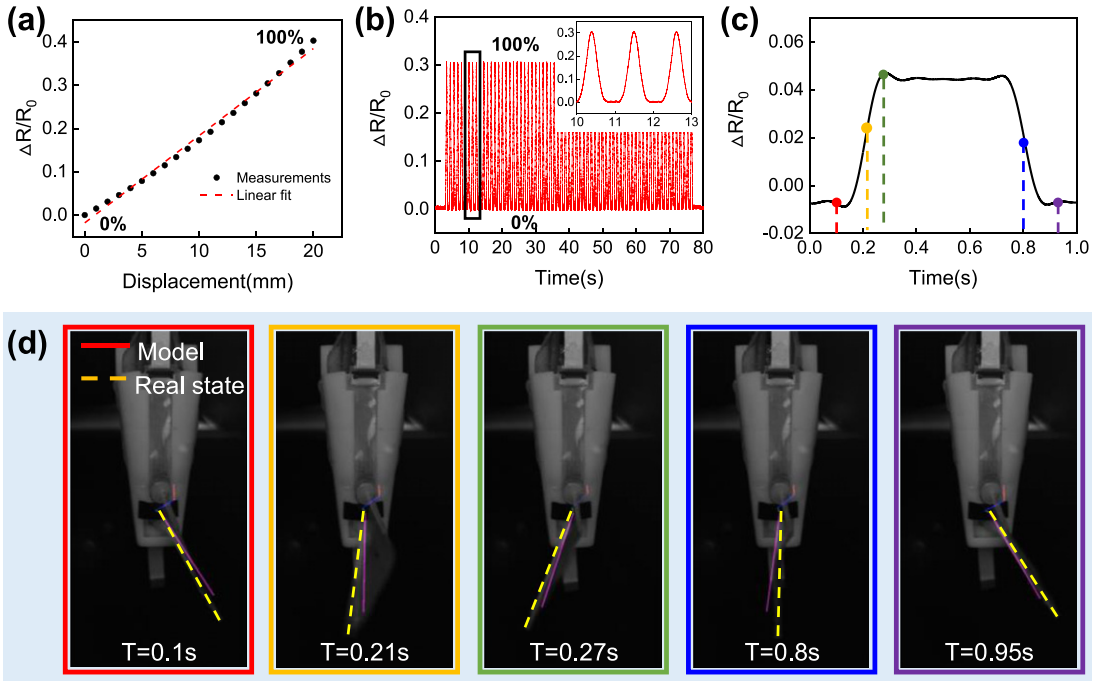

Figure 7. Finlet kinematic feedback with the liquid metal stretch sensor. (a) Performance of the liquid metal stretch sensor. The black dots represent the sensor data and the dotted red line represents a linear fit. (b) A repeating test shows that the stretch sensor maintains high reliability after stretching and releasing 80 times. (c) Resistance as a function of time. The results show the fin ray swing motions. (d) Image sequences of the robotic finlet taken by a high-speed camera corresponding to the colored dashed lines in (c), where the real-time positions (yellow dotted line) and the sensor feedback (purple solid line) are shown.

and vertical directions), proving that the robotic finlet can successfully sense the direction of the spatial force.

On the contrary, the increase of the cross-sectional area of the micro-channel will decrease its change in resistance. According to figure 3(a), the micro-channel of the sensor will be pressed when the fins are subjected to an external force. In contrast, the micro-channel of the sensor in the opposite direction will be raised.

The ability of the robotic finlet to perceive complex flow fields was also explored (figure 9). After the water has passed through the D-shaped pillar, the double-row vortex street will periodically fall off downstream. The robotic finlet was placed in the Kármán vortex street downstream of the D-shaped pillar, and the DPIV method was applied to capture the process of the Kármán vortex street sweeping across the fin surface with a high-speed camera while collecting the sensing resistance (figure 9(a)).

Figures 9(b)–(d) show that when the Kármán vortex street flows through the robotic finlet, the resistance of each sensor produces periodic fluctuations with a certain phase difference, and the period of the fluctuation is approximately equal to the period when the Kármán vortex street falls off. When the Kármán vortex street is at the front of the finlet (figure 9(b)), the resistance of sensor 1 increases (the black dashed line in figure 9(a)). Then the Kármán vortex flows to the back, and the flexible fin membrane receives the lateral force, generating a pulling force on both the fin rays (figure 9(c)) and thereby increasing the resistance of sensors 2 and 5 (the black solid line in figure 9(a). Finally, when the Kármán vortex flows to the rear of the finlet (figure 9(d)), the resistance of sensor 6 is increased by the lateral force (the black dot-dashed line in figure 9(a)). Therefore, the phase difference between the value change of the sensors represents the entire process of the Kármán vortex street flowing through the robotic finlet, indicating that the robotic finlet has the ability to perceive the surrounding complex flow field.

4. Discussion

4.1. Printed liquid metal for finlet sensing

An array of liquid metal soft sensors can be fabricated by liquid metal printing technology (figure 2). The results show that the soft sensors exhibit a high sensitivity and can respond to a minimum external force of 50 mN (figure 4(e)). The liquid metal soft sensors use the principle of resistance change caused by the deformation of the micro-channel to realize sensing [42]. The sensitivity of the liquid metal sensors is related to the cross-sectional area of the liquid metal micro-channel and the length of the micro-channel per unit area. An increase in the length of the micro-channel leads to a complex pattern. In this study, liquid metal printing technology allows the printing of complex patterns and sensing with a minimum line width and line spacing of 100 μm on a two-dimensional plane.

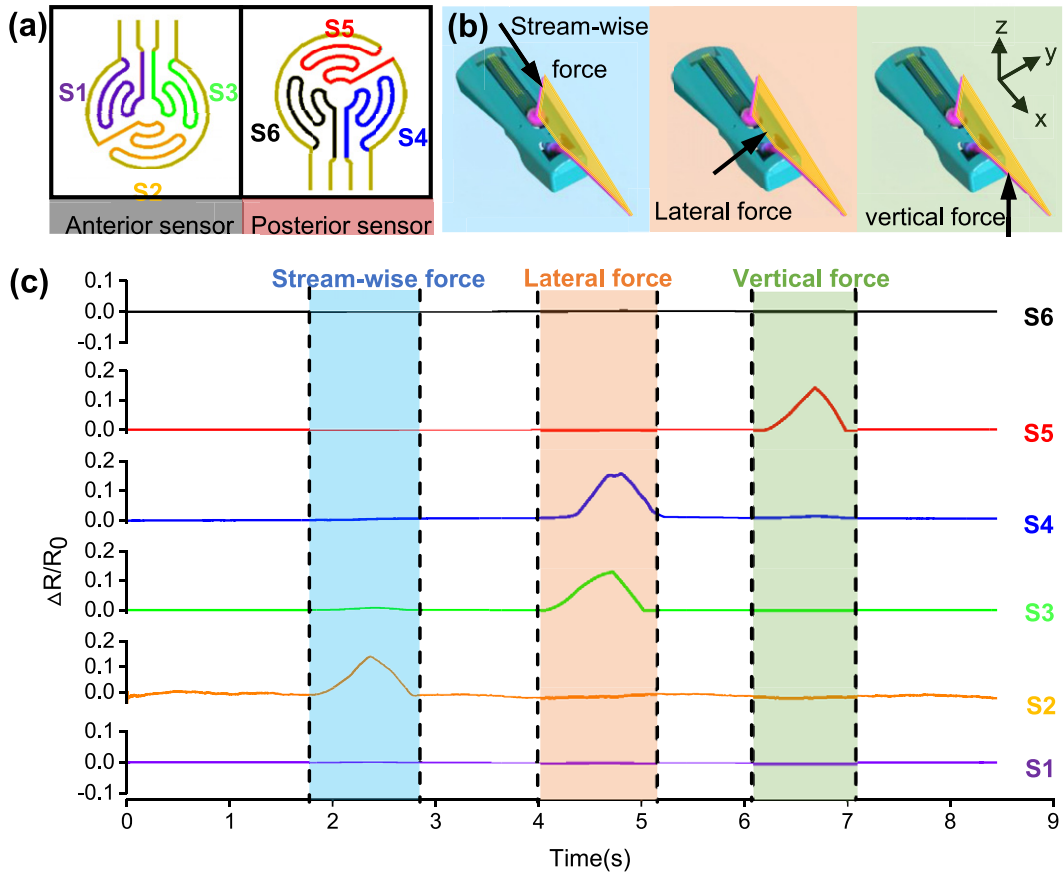

Figure 8. Flow-sensing results for the prototype robotic finlet. The robotic finlet has two flow-sensing elements (anterior and posterior fin rays). (a) Sensor pattern of two flow sensors (S1–S6) corresponding to the result in (c). (b) An illustration of force applied to the fin ray. (c) Result of resistance output as a function of time. Different sensory outputs under different force inputs are shown.

The biomimetic robotic fin ray integrated with an array of the liquid metal soft sensors on the substrate can sense external forces in multiple directions (figures 4(a)–(c)). When the fin ray is subjected to forces in different directions along the plane, the micro-channels of the soft sensor at the corresponding positions underneath the fin ray will be indented. The direction of the force can be determined from the resistances of the outputs of the three soft sensors. Here, we have verified this conclusion by applying external forces in three different directions to the fin ray.

In [33] a superficial neuromast sensory system was introduced. The robotic finlet has a sensory system composed of both a flow sensor and a proprioception sensor. The membrane has a unique morphology that distinguishes the sensory principle of the currently proposed finlet and the previous beam-like sensors, as the soft membrane can amplify the sensory output.

Inspection of figures 4(a) and (c) showed an interesting phenomenon. When the micro-channel was pressed, the increase in the resistance of sensor 1 ($\triangle R/R$ from 0 to 0.3) is much larger than the decrease in resistance ($\triangle R/R$ from 0 to −0.03) when it is pulled. This probably because the reduction in the cross-sectional area of the micro-channel caused by the pressure is larger than the increase in the cross-sectional area caused by the tension under the same force. Further mathematical models and more systematic experiments will be conducted in future work.

Accurate perception of the external flow field by the fins is essential if fish are to swim efficiently. When the finlet can perceive water flow, the fish finlets can actively adjust movement with regard to the surrounding flow and improve propulsive performance accordingly. Having both actuation and perception in one system would endow the robot with this ability.

4.2. The function of the morphological features of the finlet

The finlet has a unique overhang structure at its posterior. The anatomy shows that the finlet fin ray has a radiating pattern extending from a more concentrated base to the exterior space [6]. Previous studies have hypothesized that the suspended structure may enhance the effect of directing the surrounding flow during swimming [1–3]. Lauder *et al* showed that a similar prototype structure could reduce the lateral force generated during swimming [6]. The

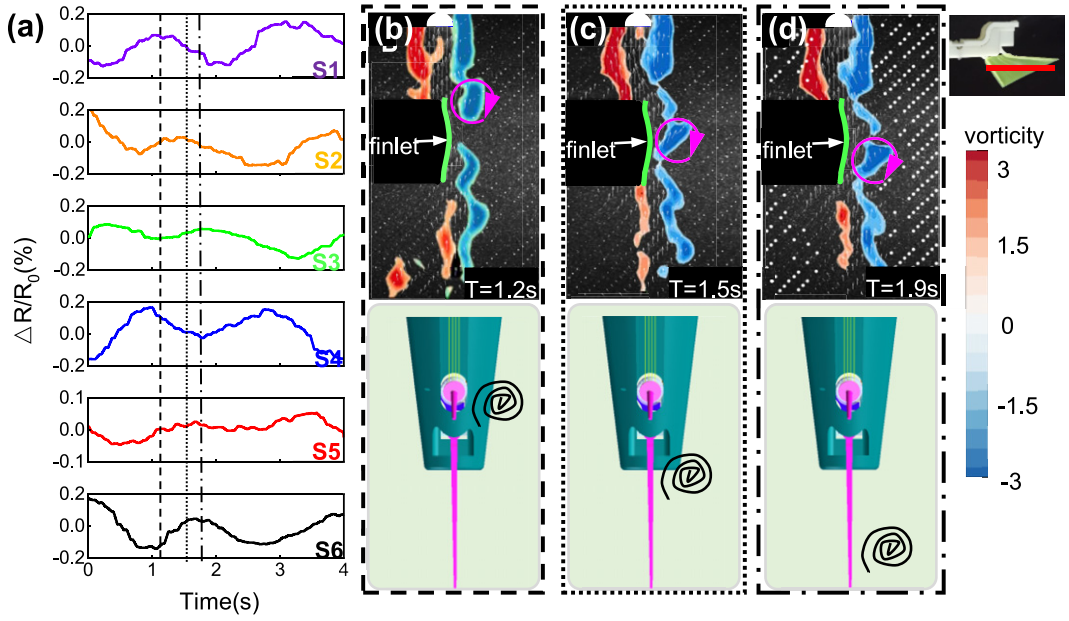

Figure 9. Vortex-sensing performance of the finlet flow sensor. (a) Sensor data for vortex sensing. The different colored curves represent the resistance change of the sensor corresponding to figure 7(a). (b)–(d) The DPIV result of a Kármán vortex street applied on the finlet corresponding to the time of $T = 1.2$ s, 1.5 s and 1.9 s in (a). Parts (a)–(c), respectively, show the DPIV images when the vortex reaches the first fin ray, the middle position of the finlet surface and the end position of the second fin ray. A pink circle in DPIV images and a black helix shape in the schematics indicates the vortex. The red line in the top right corner indicates the laser plane.

swinging movement of the finlet reaches 120°, which is biologically relevant to the range of observed animal swimming [5]. Previous studies indicate that during the swimming of fish the finlet can actively change its angle to redirect the surrounding flow [6]. Our robotic prototype can actively swing with a proprioceptive function, providing an effective experimental platform for more in-depth research on finlets.

We found that the robotic finlet composed of two orthogonally distributed fins is an essential underwater perception system that can sense forces from streamwise, lateral and vertical directions. Although there are a few studies on biomimetic sensing systems, for example bionic seal beards [28] and biomimetic fish lateral line hairs [43–46], these systems are limited to the perception of water flow in a two-dimensional plane. For the finlet prototype, each fin ray can perceive force in two-dimensional space. The standing anterior fin ray makes it possible to detect any flow wave from the x–y plane, while the posterior fin ray can detect the flow wave on the y–z plane. In particular, the two orthogonal fin rays at the anterior and posterior of the finlet build a Cartesian coordinate system similar to that of spatial orthogonality; thus, the perception of flow field information in three-dimensional space can be realized by two fin rays.

Beam-like sensors such as whiskers can be simplified as a rod when they encounter the surrounding flow. A fin ray alone can be regarded as a beam-like sensor. Note that the finlet has a soft fin membrane that connects both of the fin rays—this soft membrane provides an additional component that interacts with the flow. We conducted additional experiments to show the effect of the soft fin membrane. The existence of the fin membrane increases the area of interaction between the finlet and the water flow. Due to the connection of the fin membrane and the fin ray, forces detected by the membrane could be transmitted to the fin ray, causing an enlarged deformation of the flow sensor. Therefore, the existence of the fin membrane would also benefit in sensing motion of the posterior fin ray.

One limitation of the current study is that the fin membrane couples the sensing of the anterior and posterior fins. The biomimetic fin membrane is made of soft silicone material, and its forces and deformation in the flow field are complicated. Besides, the sensor that senses the flow field is not distributed in the fin membrane. Thus, we cannot decouple the two fin sensors for sensing the water flow environment from a tilted angle or from an arbitrary direction. We will distribute sensors on the fin membrane in the future.

Tuna have multiple finlets with different moving angles and morphologies [1, 5, 6]. Applying multiple robotic finlets to a robotic fish could be a new approach to unveil the hydrodynamic function of finlets as well as sensing the surrounding flow. In the future, we will combine the robotic finlets with an undulatory robotic fish body and systematically study this question.

According to flow and vortex sensing, this prototype shows promising underwater locomotor and sensing ability. Due to the limited resolution of liquid metal printing, more effort is needed to improve the prototype for high-precision measurements. For example, how do the micro-channels of liquid metal and the oxide on the surface of liquid metal affect the resistance? More quantitative hydrodynamic experiments remain to be conducted in future studies.

Acknowledgments

We thank Zhexin Xie and Wenbo Liu for their contributions to this article. This work was supported by the National Science Foundation support projects, China (Grant No. 91848206), in part by National Key R & D Program of China (Grant No. 18YFB1304600) and National Science Foundation support projects 91848105, 61822303, 61633004. Wenguang Sun is supported by the Academic Excellence Foundation of Beihang University for PhD Students.

Data availability statement

All data that support the findings of this study are included within the article (and any supplementary files).

ORCID iDs

Wen Li https://orcid.org/0000-0002-1498-3103

References

[1] Nauen J C and Lauder G V 2000 Locomotion in scombrid fishes: morphology and kinematics of the finlets of the chub mackerel *Scomber japonicus J. Exp. Biol.* **203** 2247–59
[2] Nauen J C and Lauder G V 2001 Locomotion in scombrid fishes: visualization of flow around the caudal peduncle and finlets of the chub mackerel *Scomber japonicus J. Exp. Biol.* **204** 2251–63
[3] Nauen J C and Lauder G V 2001 Three-dimensional analysis of finlet kinematics in the chub mackerel (*Scomber japonicus*) *Biol. Bull.* **200** 9–19
[4] Walters V 1962 Body form and swimming performance in the scombroid fishes *Am. Zoologist* **2** 143–9
[5] Wang J, Wainwright D K, Lindengren R E, Lauder G V and Dong H 2020 Tuna locomotion: a computational hydrodynamic analysis of finlet function *J. R. Soc. Interface* **17** 20190590
[6] Wainwright D K and Lauder G V 2020 Tunas as a high-performance fish platform for inspiring the next generation of autonomous underwater vehicles *Bioinspir. Biomim.* **15** 035007
[7] Buckland-Nicks J A, Gillis M and Reimchen T E 2012 Neural network detected in a presumed vestigial trait: ultrastructure of the salmonid adipose fin *Proc. R. Soc.* B **279** 553–63
[8] Thorsen D H and Hale M E 2007 Neural development of the zebrafish (*Danio rerio*) pectoral fin *J. Comp. Neurol.* **504** 168–84
[9] Buckland-Nicks J A 2016 New details of the neural architecture of the salmonid adipose fin *J. Fish Biol.* **89** 1991–2003
[10] Williams R IV, Neubarth N and Hale M E 2013 The function of fin rays as proprioceptive sensors in fish *Nat. Commun.* **4** 1729
[11] Aiello B R, Stewart T A and Hale M E 2016 Mechanosensation in an adipose fin *Proc. R. Soc.* B **283** 20152794
[12] Aiello B R, Westneat M W and Hale M E 2017 Mechanosensation is evolutionarily tuned to locomotor mechanics *Proc. Natl Acad. Sci. USA* **114** 4459–64
[13] Williams R t and Hale M E 2015 Fin ray sensation participates in the generation of normal fin movement in the hovering behavior of the bluegill sunfish (*Lepomis macrochirus*) *J. Exp. Biol.* **218** 3435–47
[14] Flammang B E and Lauder G V 2013 Pectoral fins aid in navigation of a complex environment by bluegill sunfish under sensory deprivation conditions *J. Exp. Biol.* **216** 3084–9
[15] Hardy A R, Steinworth B M and Hale M E 2016 Touch sensation by pectoral fins of the catfish *Pimelodus pictus Proc. Biol. Sci.* **283** 20152652
[16] Hardy A R and Hale M E 2020 Sensing the structural characteristics of surfaces: texture encoding by a bottom-dwelling fish *J. Exp. Biol.* **223** jeb227280
[17] Ono R D 1979 Sensory nerve endings of highly mobile structures in two marine teleost fishes *Zoomorphologie* **92** 107–14
[18] Ono R D and Poss S G 1982 Structure and innervation of the swim bladder musculature in the weakfish, *Cynoscion regalis* (Teleostei: Sciaenidae) *Can. J. Zool.* **60** 1955–67
[19] Wan Y, Wang Y and Guo C F 2017 Recent progresses on flexible tactile sensors *Mater. Today Phys.* **1** 61–73
[20] Frutiger A, Muth J T, Vogt D M, Mengüç Y, Campo A, Valentine A D, Walsh C J and Lewis J A 2015 Capacitive soft strain sensors via multicore-shell fiber printing *Adv. Mater.* **27** 2440–6
[21] Hammock M L, Chortos A, Tee B C-K, Tok J B-H and Bao Z 2013 25th anniversary article: The evolution of electronic skin (e-skin): a brief history, design considerations, and recent progress *Adv. Mater.* **25** 5997–6038
[22] Joo Y, Yoon J, Ha J, Kim T, Lee S, Lee B, Pang C and Hong Y 2017 Highly sensitive and bendable capacitive pressure sensor and its application to 1 V operation pressure-sensitive transistor *Adv. Electronic Mater.* **3** 1600455
[23] Kaltenbrunner M *et al* 2013 An ultra-lightweight design for imperceptible plastic electronics *Nature* **499** 458–63
[24] Li T, Luo H, Qin L, Wang X, Xiong Z, Ding H, Gu Y, Liu Z and Zhang T 2016 Flexible capacitive tactile sensor based on micropatterned dielectric layer *Small* **12** 5042–8
[25] Lipomi D J, Vosgueritchian M, Tee B C-K, Hellstrom S L, Lee J A, Fox C H and Bao Z 2011 Skin-like pressure and strain sensors based on transparent elastic films of carbon nanotubes *Nat. Nanotechnol.* **6** 788–92
[26] Mannsfeld S C B, Tee B C-K, Stoltenberg R M, Chen C V H-H, Barman S, Muir B V O, Sokolov A N, Reese C and Bao Z 2010 Highly sensitive flexible pressure sensors with microstructured rubber dielectric layers *Nat. Mater.* **9** 859–64
[27] Deer W and Pounds P E I 2019 Lightweight whiskers for contact, pre-contact, and fluid velocity sensing *IEEE Robot. Autom. Lett.* **4** 1978–84
[28] Gul J Z, Su K Y and Choi K H 2018 Fully 3D printed multi-material soft bio-inspired whisker sensor for underwater-induced vortex detection *Soft Robot.* **5** 122–32
[29] Takei K, Yu Z, Zheng M, Ota H, Takahashi T and Javey A 2014 Highly sensitive electronic whiskers based on patterned carbon nanotube and silver nanoparticle composite films *Proc. Natl Acad. Sci. USA* **111** 1703–7

[30] Chou S-W *et al* 2017 A molecular basis for water motion detection by the mechanosensory lateral line of zebrafish *Nat. Commun.* **8** 2234
[31] Coombs S and Van Netten S 2005 The hydrodynamics and structural mechanics of the lateral line system *Fish Biomechanics* (New York: Elsevier) pp 103–39
[32] Schmitz A, Bleckmann H and Mogdans J 2008 Organization of the superficial neuromast system in goldfish, *Carassius auratus J. Morphol.* **269** 751–61
[33] Ristolainen A 2016 Hydromast: a bioinspired flow sensor with accelerometers *Conf. Biomimetic and Biohybrid Systems* (Berlin: Springer)
[34] Lauder G V, Madden P G A, Tangorra J L, Anderson E and Baker T V 2011 Bioinspiration from fish for smart material design and function *Smart Mater. Struct.* **20** 094014
[35] Wen L, Wang T M, Wu G H and Liang J H 2012 Hydrodynamic investigation of a self-propelled robotic fish based on a force-feedback control method *Bioinspir. Biomim.* **7** 036012
[36] Wen L, Wang T, Wu G and Liang J 2013 Quantitative thrust efficiency of a self-propulsive robotic fish: experimental method and hydrodynamic investigation *IEEE/ASME Trans. Mechatron.* **18** 1027–38
[37] Wen L, Weaver J C and Lauder G V 2014 Biomimetic shark skin: design, fabrication and hydrodynamic function *J. Exp. Biol.* **217** 1656–66
[38] Sun W, Liu Z, Ren Z, Wang G, Yuan T and Wen L 2020 Linear acceleration of an undulatory robotic fish with dynamic morphing median fin under the instantaneous self-propelled condition *J. Bionic Eng.* **17** 241–53
[39] Wen L, Ren Z, Di Santo V, Hu K, Yuan T, Wang T and Lauder G V 2018 Understanding fish linear acceleration using an undulatory biorobotic model with soft fluidic elastomer actuated morphing median fins *Soft Robot.* **5** 375–88
[40] Ren Z, Yang X, Wang T and Wen L 2016 Hydrodynamics of a robotic fish tail: effects of the caudal peduncle, fin ray motions and the flow speed *Bioinspir. Biomim.* **11** 016008
[41] Zhu J, White C, Wainwright D K, Di Santo V, Lauder G V and Bart-Smith H 2019 Tuna robotics: a high-frequency experimental platform exploring the performance space of swimming fishes *Sci. Robot.* **4** eaax4615
[42] Yong-Lae Park P, Bor-Rong Chen C and Wood R J 2012 Design and fabrication of soft artificial skin using embedded microchannels and liquid conductors *IEEE Sensors J.* **12** 2711–8
[43] Asadnia M, Kottapalli A G P, Miao J, Warkiani M E and Triantafyllou M S 2015 Artificial fish skin of self-powered micro-electromechanical systems hair cells for sensing hydrodynamic flow phenomena *J. R. Soc. Interface* **12** 20150322
[44] Wolf B J, Morton J A S, MacPherson W N and van Netten S M 2018 Bio-inspired all-optical artificial neuromast for 2D flow sensing *Bioinspir. Biomim.* **13** 026013
[45] Yang Y, Klein A, Bleckmann H and Liu C 2011 Artificial lateral line canal for hydrodynamic detection *Appl. Phys. Lett.* **99** 023701
[46] Yang Y, Nguyen N, Chen N, Lockwood M, Tucker C, Hu H, Bleckmann H, Liu C and Jones D L 2010 Artificial lateral line with biomimetic neuromasts to emulate fish sensing *Bioinspir. Biomim.* **5** 016001